

Influence of surface morphology on surface states for Cu on Cu(111)

Th. Fauster, Ch. Reuß, I. L. Shumay, and M. Weinelt
Lehrstuhl für Festkörperphysik, Universität Erlangen-Nürnberg, D-91054 Erlangen, Germany

F. Theilmann and A. Goldmann
Fachbereich Physik, Universität Kassel, D-34131 Kassel, Germany
 (Received 14 December 1999)

We have exploited angle-resolved one-photon photoemission, two-photon photoemission, and spot-profile analysis of low-energy electron diffraction to monitor the influence of surface morphology on the occupied and empty surface states observed at Γ on Cu(111). Surface morphology changes were induced by homoepitaxial growth of Cu on Cu(111). A simple model of electron localization on terraces successfully explains energy shifts and linewidth broadening of both surface states. Obviously, surface states may be used as sensitive probes of terrace-width distributions and other structural properties.

I. INTRODUCTION

Theoretical calculations of the surface electronic structure usually assume a perfect, well-ordered surface at zero temperature. These results are compared to photoemission measurements on real surfaces containing many defects at finite temperature.¹ The proper extrapolation of the experimental results to zero defect concentration and zero temperature should yield the energies and linewidths of the excited states that may be compared to the theoretical calculations. In order to achieve this goal the influence of defects on the photoemission spectra has to be studied.

Some progress in this direction has been made^{2,3} and in this contribution we make a quantitative correlation between the surface morphology as observed by spot-profile analysis low-energy electron diffraction (SPALEED) and photoemission results for surface states. The system Cu on a Cu(111) surface was chosen, because there exist an occupied surface state as well as an unoccupied image-potential state. The first is observed by regular photoemission experiments,¹ whereas two-photon photoemission experiments⁴ can detect both states with high resolution.

The growth of Cu on Cu(111) has been studied by several groups before.⁵⁻¹¹ Deposition of copper at low temperatures (90 K) leads to a rough surface, which may be described rather well by a completely random growth.⁵ Reports of a reentrant layer-by-layer growth⁶⁻⁸ could not be confirmed in later studies.^{9,11} The experimental indications for the layer-by-layer growth were quoted to be rather weak.¹¹ In the present paper we find no indications for a layer-by-layer growth mode for Cu on Cu(111) and the results can be interpreted consistently assuming a random growth mode. Further support comes from scanning tunneling microscopy studies¹² that report a rather large value of 0.22 eV for the Ehrlich-Schwobel barrier. This hinders the jump of atoms onto lower terraces, which is the limiting step for layer-by-layer growth.

This paper describes first the experimental details. The results and discussion are presented in several sections. Some relationships are independent of coverage and annealing temperature. The coverage dependence at fixed tempera-

ture can be interpreted consistent with the random growth mode. A quantitative data analysis using the SPALEED results is attempted before the final discussion and conclusions are given.

II. EXPERIMENT

The results were obtained with two different ultrahigh vacuum systems. The experimental details of the SPALEED and photoemission apparatus have been described before.³ The measurement of both surface states was done by two-photon photoelectron spectroscopy (2PPE).^{4,13} A first laser pulse in the ultraviolet range excites an electron from an initial state into an intermediate state above the Fermi level. A second photon in the infrared regime lifts the electron above the vacuum level E_{vac} so it may leave the surface and can be detected in an energy analyzer. Scanning the spectrum with the analyzer yields the energy and linewidth of the state.

The sample preparation was done on two different crystals following identical procedures.³ Copper coverages up to 5 ML (monolayers) were deposited at 90 K. The samples were annealed to 110 K to avoid Ostwald ripening at the measurement temperature of 90 K. Subsequently, the samples were stepwise annealed up to 300 K. At higher annealing temperatures spectra identical to those from a clean well-annealed surface were observed. In order to correlate the photoemission results with the SPALEED work, we had to rely on the photoemission spectra of the occupied surface state, which could be obtained at both locations. Additional input came from the annealing temperatures, the coverages, however, were not calibrated in the SPALEED experiments.

The photoemission experiments for the occupied surface state ($n=0$) employed the Ar I resonance line. For the determination of the linewidth the Ar I doublet was decomposed and an appropriate background was subtracted. A correction for the experimental resolution was found to be unnecessary and the measured full width at half maximum (FWHM) is given for the $n=0$ state. The 2PPE spectra were fitted by Lorentzians convoluted with a Gaussian for the overall experimental resolution of 40 meV.¹⁴ The width of the Lorentzian is given for the linewidth of the $n=1$ image-

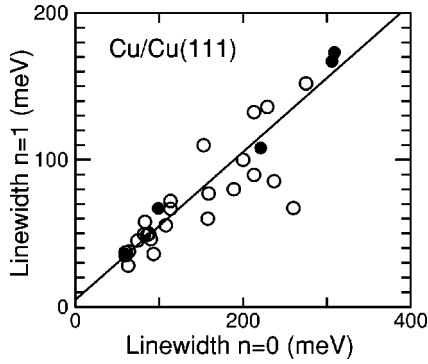


FIG. 1. Linewidth of the $n=1$ image-potential state versus the linewidth of the $n=0$ occupied surface state. Filled symbols denote data obtained at 110 K, open symbols mark higher annealing temperatures.

potential state. In order to avoid additional broadening due to direct two-photon processes, the spectra were taken with the probe pulse sufficiently delayed after the pump pulse.¹⁵

III. RESULTS

A. Relationships independent of coverage and annealing temperature

Figure 1 shows a linear relationship between the linewidth Γ_1 of the $n=1$ state and the linewidth Γ_0 of the occupied surface state for various coverages and annealing temperatures. The slope is 0.52 for the data obtained after annealing to 110 K (filled symbols). A value of 0.50 is obtained, when all the data points are included. Similar observations have been made for occupied surface states at different points of the surface Brillouin zone on Cu(111) and were related to the reciprocal ratio of the effective masses.^{2,3} On the smooth Cu(111) surface both surface states studied in this paper can be described by free-electronlike bands with energies $E_n(k_{\parallel}) = E_n(0) + \hbar^2 k_{\parallel}^2 / 2m_n^*$ as a function of parallel momentum k_{\parallel} . The occupied surface state has an effective mass $m_0^* = 0.41 m_e$ where m_e denotes the free-electron mass.¹⁶⁻¹⁸ For the first image-potential state we find $m_1^*/m_e = 1.2 \pm 0.1$. This number is slightly larger than the value 1.0 ± 0.1 reported before.¹⁹ However, the energetic proximity of the image-potential state to the upper edge of the band gap favors the larger value in agreement with model calculations²⁰ and observations for Ag(111) with a similar electronic surface structure.²¹ Using these numbers we obtain the reciprocal ratio of the effective masses of the two surface states to 0.34, somewhat lower than the experimental value at around 0.5.

The relation between the energy E_0 and the linewidth Γ_0 (FWHM) of the occupied surface state is shown in Fig. 2. The data for 110 K (filled circles) agree well with the data for higher annealing temperatures (open circles). The data of Theilmann *et al.* (diamonds, Ref. 3) were shifted downward by 20 meV to achieve better correspondence for smooth surfaces and show a significantly larger slope of 0.35 compared to the other data points that are fitted by a slope of 0.20 independent of temperature. Noting that the data are obtained for various coverages and annealing temperatures, we conclude that the surface morphology influences the energy and linewidth of the $n=0$ state through the same mechanism.

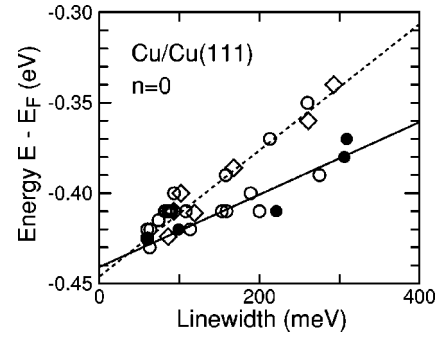


FIG. 2. Energy of occupied surface state as a function of linewidth. Filled symbols are data for 110 K, open circles correspond to annealed films. The data from Theilmann *et al.* (Ref. 3) are shifted down by 20 meV and marked by diamonds.

The same trend is followed by similar data for the $n=1$ image-potential state presented in Fig. 3. The data cover a wide range of coverages and annealing temperatures and show a clear linear correlation between linewidth and energy of the image-potential state. The energy relative to the Fermi energy E_F for the $n=1$ state decreases with increasing linewidth, because the work function decreases strongly with increasing surface roughness.²² Using the vacuum level as a reference the energy of the image-potential states actually increases with increasing linewidth as observed for the $n=0$ state in Fig. 2.

For the interpretation of the relationship between energy shifts and linewidth we assume that the surface is covered by islands with a normalized distribution of terrace lengths L of the following form²³

$$P(L) = \frac{1}{\langle L \rangle} \frac{\nu^\nu}{(\nu-1)!} \left(\frac{L}{\langle L \rangle} \right)^{\nu-1} \exp\left(-\nu \frac{L}{\langle L \rangle}\right). \quad (1)$$

The mean terrace length is denoted by $\langle L \rangle$ and the parameter $\nu = (\langle L \rangle / \sigma)^2$ determines the standard deviation σ or the width of the terrace length distribution. Following the previous discussion in this section, we assume that the observed states can be described as free electrons with an effective mass m^* . Upon localization on a terrace of width L the energy increases by an amount

$$E = \frac{\hbar^2 \pi^2}{2m^* L^2} = \varepsilon(L). \quad (2)$$

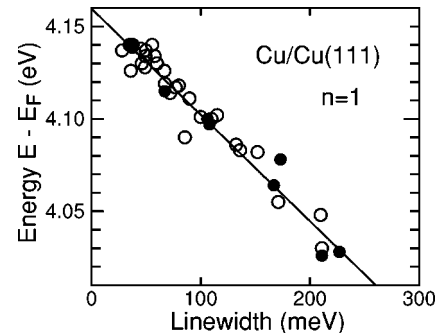


FIG. 3. Energy of $n=1$ image-potential state as a function of linewidth. Filled symbols are data for 110 K, open circles correspond to annealed films.

Combining Eqs. 1 and 2 we can immediately calculate the mean energy shift

$$\langle E \rangle = \int_0^\infty E(L)P(L)dL = \varepsilon(\langle L \rangle) \frac{(\nu-3)!}{(\nu-1)!} \nu^2 \quad (3)$$

and the second moment

$$\langle E^2 \rangle = \int_0^\infty [E(L)]^2 P(L)dL = \varepsilon(\langle L \rangle)^2 \frac{(\nu-5)!}{(\nu-1)!} \nu^4 \quad (4)$$

from which the mean-square deviation can be obtained as an approximation for the linewidth

$$\Gamma \approx \sqrt{\langle E^2 \rangle - \langle E \rangle^2} = \varepsilon(\langle L \rangle) \frac{\sqrt{(\nu-1)!(\nu-5)! - (\nu-3)!^2}}{(\nu-1)!} \nu^2. \quad (5)$$

Within this model the surface morphology enters only through the parameter ν and the average terrace length $\langle L \rangle$. Therefore, it follows from Eqs. (5) and (2) immediately, that the linewidths for different free-electronlike states are indirectly proportional to the effective masses m^* as observed in Fig. 1. The relationship between energy shift $\langle E \rangle$ and linewidth Γ is obtained from Eqs. (3) and (5). The integral in Eq. (4) exists only for $\nu \geq 5$ with a minimum value for $\langle E \rangle / \Gamma = 0.45$ for $\nu = 5$. This is of the right order of magnitude, but still considerably larger than the experimental values that range between 0.20 and 0.35 in Fig. 2. Lower values of ν would bring the proportionality factor closer to the experimental values, but the SPALEED results presented in Sec. III C are compatible with $\nu = 5$. The main reason for the discrepancy is the use of Eq. (2) for arbitrarily small terrace widths L . This leads to the divergence of the integrals in Eqs. (3) and (4) for small ν corresponding to an overestimate of the linewidth in Eq. (5). The electrons on the terraces are confined by a potential of finite height, which could be approximated by a finite value for the lower limit in the integrals. For calculations with a finite lower integration limit, we would need, however, a reasonable estimate for the barrier height and for $\langle L \rangle$. It should be noted, that the main conclusions of this section may be obtained for any distribution of the form $P(L) = p(L/\langle L \rangle)/\langle L \rangle$. The distribution affects only the numerical factors retaining the energy dependence $\varepsilon(\langle L \rangle)$. The form of Eq. (1) is physically meaningful,²³ provides sufficient flexibility through the parameter ν , and can be evaluated analytically.

B. Coverage dependence at 110 K

Figure 4 presents two-photon photoemission spectra for the $n=1$ image-potential state as a function of Cu coverage deposited at 110 K on Cu(111). The coverages were obtained using a calibrated quartz microbalance with an estimated error of 10%. The intensity is scaled arbitrarily but decreases with coverage as can be inferred from the noise level of the data. A significant broadening of the peak with increasing coverage can be seen accompanied by a downward shift in energy relative to E_F . The line shape analysis of the spectra yields the intrinsic linewidth and energy position of the peaks. These data for the $n=1$ states and the corresponding results for the $n=0$ states are discussed in this section.

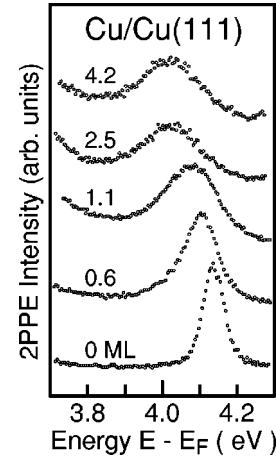


FIG. 4. Two-photon photoemission spectra for the $n=1$ image-potential state as a function of Cu coverage on Cu(111) at 110 K.

The top panel of Fig. 5 shows a linear relationship between the linewidth Γ of the $n=1$ state and the Cu coverage Θ on Cu(111) at 110 K for coverages below 2.5 ML. For the $n=0$ state the data range is limited at higher coverages due to the large width of the spectra and the cutoff corresponding to the Fermi energy. For the $n=1$ state there seems to be a saturation around 220 meV at higher coverages. A possible explanation would be the energy limit when the model [Eq. (2)] would be modified using a finite barrier height. A similar argument would apply also to the $n=0$ state. However, this cannot be confirmed because of the limited range of the available experimental data.

The linewidth increase upon Cu deposition, is according to Fig. 5, proportional to the Cu coverage. From Eqs. (2) and (5) we obtain the following dependence on coverage (in ML) of the mean terrace width

$$\langle L \rangle = \lambda \Theta^{-1/2}. \quad (6)$$

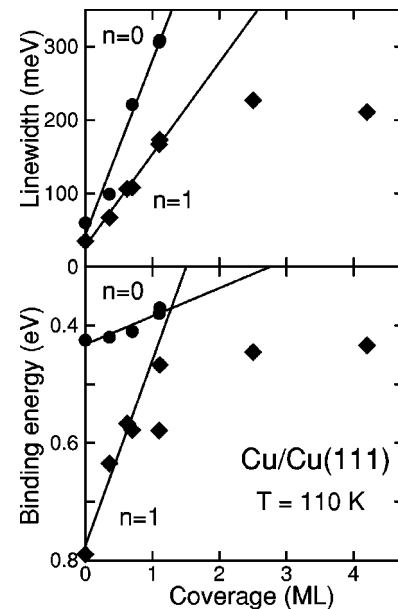


FIG. 5. Linewidths and binding energies for the $n=0$ and $n=1$ states as a function of Cu coverage on Cu(111) at 110 K. The binding energies are relative to E_F and E_{vac} for the $n=0$ and $n=1$ states, respectively.

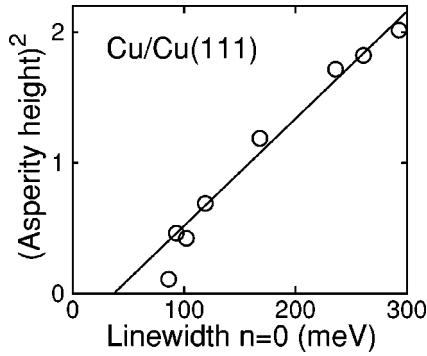


FIG. 6. Square of the asperity height plotted against the linewidth of the $n=0$ state. The solid line is a linear fit omitting the data point with the smallest asperity height.

This corresponds to the expectation for random growth, where the mean area of the terraces is proportional to $1/\Theta$. The model developed in Sec. III A enables us now to determine the mean terrace width from the analysis of the linewidth data. Quantitative evaluation of Eq. (5) assuming $\nu = 5$ gives $\lambda = 42$ Å and 34 Å from the data of Fig. 5 for the $n=0$ and $n=1$ state, respectively. These values should be taken as a rough estimate, because of the uncertainty in the choice of ν and the neglect of a finite barrier height. In Sec. III C the results by diffraction techniques compare rather well with our results from linewidth analysis of photoemission data.

Applying these results to the energy shift given by Eq. (3) should yield also a linear relationship as a function of coverage. The data in the bottom panel of Fig. 5 support this prediction for coverages below 2.5 ML. For the $n=0$ state a small increase is seen, making the determination of the functional relation difficult. As noted already in Sec. III A the energy shift is rather small compared to the increase in linewidth, which makes the discussion of the linewidth more reliable. For the $n=1$ state the binding energy relative to the vacuum level decreases with coverage. The energy relative to E_F decreases,²² because the work function decreases strongly with Cu coverage.²² This makes a quantitative interpretation of the energy of the $n=1$ state within the present model difficult.

C. Relation to surface morphology

In the preceding sections we have analyzed the energies and linewidths from the photoemission spectra within a rather simple model. We will now relate these findings to the structural results obtained by SPALEED^{3,5} or thermal energy He scattering.¹¹

The vertical roughness of the surface is measured by the asperity height Δ in units of the layer height.⁵ In Fig. 6 the data from Theilmann *et al.*³ are plotted quadratically as a function of the linewidth of the $n=0$ surface state. The fit (neglecting the data point for the smallest asperity height, i.e., the smoothest surface) shows a linear relationship. The intrinsic linewidth for a smooth surface ($\Delta=0$) is obtained to 37 meV, in good agreement with Fig. 5 and previous work.² Combining the results of Figs. 5 and 6 we obtain $\Delta^2 \approx 2\Theta$. This relationship is expected for the random growth model as found in the preceding section from the

linewidth analysis and as verified for Ag/Ag(111).²³ The proportionality factor should, however, be 1 for the ideal random growth.^{5,23} This discrepancy might be due to the combination of results from two different experiments and samples. In particular, the measurements of Theilmann *et al.*³ included data for annealed samples, which lead to a decrease of the asperity height⁵ as well as the linewidth.

The diffraction techniques permit a quantitative determination of the mean terrace width from the analysis of the spot profiles. The previously published values of the step atom density^{3,5} are not compatible with the length scales derived in this work. The original SPALEED data in Fig. 6 of Ref. 5 for 2.5 ML deposited at 135 K show a ring with a K_{\parallel} radius of $\approx 4\% \ 2\pi/a$. This is in agreement with the data for the roughest surface ($\Delta=1.42$) studied by Theilmann,²⁴ which corresponds to a sample preparation without further annealing. For random growth $\Theta = \Delta^2 = 2$ ML, which is as a lower limit compatible with the given coverage regime.^{3,24} The conversion of the ring radius to the mean terrace width [Eq. (3b) of Ref. 23] requires the knowledge of $\sigma/\langle L \rangle$ or equivalently ν . For large ν , as evidenced by a clearly developed ring, the ring radius is approximately $\pi/\langle L \rangle$. We obtain $\langle L \rangle = 12.5a = 32$ Å which can be compared to the estimates using Eq. 6 for $\Theta = 2.5$ ML. Depending on the choice for λ our values of 22 or 27 Å are in good agreement with the SPALEED result. The thermal energy He-scattering study¹¹ reports a length scale of 150 Å for 0.1 ML of Cu deposited on Cu(111) at 100 K. Our estimates from Eq. (6) yield slightly lower values of 108 and 133 Å.

The parameter $\nu = (\langle L \rangle / \sigma)^2$ describes the relation between the width σ of the terrace width distribution in terms of its mean value $\langle L \rangle$. In SPALEED measurements this corresponds to the width of the ring compared to its radius. The experimental data for Cu on Cu(111)²⁴ give a parameter in the range $\nu = 4, \dots, 7$ in good agreement with the previously assumed value of $\nu = 5$. The results of this section show, that the data analysis of the linewidths within the simple model is consistent with the full information from the results obtained by diffraction techniques.

IV. DISCUSSION

In the previous sections we have shown that the energy shift and linewidth broadening caused by deposition of Cu on Cu(111) can be described by a simple model in which the electrons are localized on the flat areas of the sample. The concept of the energy shift [Eq. (3)] has been used previously^{25,26} to explain the linewidth broadening of image-potential states due to molecular adsorbates. The success of this simple model can be explained by the fact that both energy shift and linewidth are proportional to $\varepsilon(\langle L \rangle)$ [see Eqs. (3) and (5)] for any distribution of the form $P(L) = p(L/\langle L \rangle)/\langle L \rangle$. The details of the distribution go into the numerical factors. For the occupied surface state on stepped Cu(111) surfaces the energy shift has been calculated successfully by a modified expression Eq. (3), which describes the localizing barriers within a Kronig-Penney model.^{27,28} It is interesting to note, that the energy shift of the occupied surface states on the stepped surfaces follows approximately an $\langle L \rangle^{-2}$ dependence, but the energy shifts are much larger^{27,29} than observed in the present study for rough sur-

faces (see Fig. 5 bottom). The $n=1$ image-potential state on Cu(775) on the other hand shows a binding energy shift of 50 meV.²⁹ Using the experimental relationship between energy and coverage from Fig. 5 we obtain for $\lambda=34$ Å a mean terrace width of 14 Å, in perfect agreement with the actual value for a Cu(775) surface.

The data analysis within the present model implicitly assumes an inhomogeneous broadening of the states that have different energies on different terraces. This is in contrast with experimental results, which show that the inelastic decay rate (inverse lifetime) of the $n=1$ image-potential states changes upon Cu deposition.^{30,22} In the latter study the additional broadening of the linewidth was attributed to dephasing by quasielastic scattering processes. For Cu on Cu(111) about 30% of the linewidth increase of the $n=1$ image-potential state can be attributed to the increase of the inelastic decay rate upon Cu coverage.²² For the occupied surface state the experimental distinction between contributions from inelastic and elastic scattering is not available. If we identify the quasielastic scattering processes with the inhomogeneous broadening (for the $n=1$ image-potential state only), the slope of 0.5 from Fig. 1 would be reduced to 0.35, in perfect agreement with the prediction from the ratio of the effective masses. Experimentally it is rather difficult to distinguish between homogeneous and inhomogeneous broadening. Calculations within a scattering description of the electron localization might provide further insight into this problem.²⁷

The homoepitaxial growth on the (111) surfaces of Ag and Cu has been found to be very similar.¹¹ The growth mode is determined mainly by the Ehrlich-Schwoebel barrier, which controls the rate at which deposited adatoms jump over descending step edges. Experimental values for Ag(111) and Cu(111) are 0.13 eV (Ref. 31) and 0.22 eV,¹² respectively. The lower value for silver might lead to a somewhat smoother surface morphology on Ag(111). Indeed, the coverage dependence of the mean terrace width has been measured as $\Theta^{-2/3}$ on Ag(111)²³ compared to the $\Theta^{-1/2}$ dependence for Cu(111) [Eq. (6)]. The large Ehrlich-Schwoebel barrier on Cu(111) leads to the random growth

mode observed in this work and by Meyer *et al.* (Ref. 5). The island sizes, on the other hand, are influenced by the terrace diffusion energy which has for Cu(111) a rather low value of 0.03 eV.¹¹ The corresponding value for Ag(111) is in the range from 0.097 eV (Ref. 32) to 0.12 or 0.18 eV.²³ However, the average terrace sizes do not seem to be very different for the two materials.^{11,23} The island density is for Cu(111) most likely determined by the quality of the surface, because the low diffusion energy makes an attachment to an existing step or defect more likely than the formation of a critical nucleus. This could lead to a narrower island size distribution on Cu(111) compared to Ag(111) as reflected in the values of the parameter $\nu=5$ for Cu and $\nu=2$ for Ag.²³

V. CONCLUSIONS AND OUTLOOK

A simple model of electron localization was used successfully to describe the energy shift and linewidth broadening of surface states for the homoepitaxial growth of Cu on Cu(111). In particular the linewidth broadening can be used to obtain reasonable estimates for the terrace size distribution in agreement with results from diffraction techniques. Occupied as well as unoccupied surface states can be used for the analysis and yield equivalent results. A careful investigation of the line shapes should yield further information on the terrace-width distributions and might explain the asymmetric line shapes found for some sample preparations.³ The energy shifts show only qualitative agreement with the model calculations. Work on stepped surfaces is in progress to clarify this point on surfaces with a well-defined surface morphology. For these systems theoretical calculations should be feasible which would provide further insight into the problem of homogeneous vs inhomogeneous broadening and elastic vs inelastic scattering processes.

ACKNOWLEDGMENT

This work was supported in part by the Deutsche Forschungsgemeinschaft DFG.

¹R. Matzdorf, Surf. Sci. Rep. **30**, 153 (1997).

²F. Theilmann, R. Matzdorf, G. Meister, and A. Goldmann, Phys. Rev. B **56**, 3632 (1997).

³F. Theilmann, R. Matzdorf, and A. Goldmann, Surf. Sci. **420**, 33 (1999).

⁴Th. Fauster and W. Steinmann, in *Photonic Probes of Surfaces*, Vol. 2 of *Electromagnetic Waves: Recent Developments in Research*, edited by P. Halevi (North-Holland, Amsterdam, 1995), Chap. 8, p. 347.

⁵G. Meyer, J. Wollschläger, and M. Henzler, Surf. Sci. **231**, 64 (1990).

⁶M. Henzler, Surf. Sci. **298**, 369 (1993).

⁷M. Henzler, Prog. Surf. Sci. **42**, 297 (1993).

⁸M. Henzler, T. Schmidt, and E. Z. Luo, in *The Structure of Surfaces IV*, edited by X. Xie, S. Y. Tong, and M. A. van Hove (World Scientific, Singapore, 1994), p. 619.

⁹P. C. Dastoor, J. Ellis, A. Reichmuth, H. Bullman, B. Holst, and W. Allison, Surf. Rev. Lett. **1**, 509 (1994).

¹⁰H. A. van der Vegt, J. Alvarez, X. Torrelles, S. Ferrer, and E. Vlieg, Phys. Rev. B **52**, 17 443 (1995).

¹¹W. Wulfhekel, N. N. Lipkin, J. Kliewer, G. Rosenfeld, L. C. Jorritsma, B. Poelsema, and G. Comsa, Surf. Sci. **348**, 227 (1996).

¹²M. Giesen and H. Ibach, Surf. Sci. **431**, 109 (1999).

¹³U. Thomann, I. L. Shumay, M. Weinelt, and Th. Fauster, Appl. Phys. B: Lasers Opt. **68**, 531 (1999).

¹⁴N. Fischer, S. Schuppler, Th. Fauster, and W. Steinmann, Phys. Rev. B **42**, 9717 (1990).

¹⁵I. L. Shumay, U. Höfer, Ch. Reuß, U. Thomann, W. Wallauer, and Th. Fauster, Phys. Rev. B **58**, 13 974 (1998).

¹⁶P. O. Gartland and B. J. Slagsvold, Phys. Rev. B **12**, 4047 (1975).

¹⁷B. A. McDougall, T. Balasubramanian, and E. Jensen, Phys. Rev. B **51**, 13 891 (1995).

¹⁸R. Matzdorf, G. Meister, and A. Goldmann, Phys. Rev. B **54**, 14 807 (1996).

¹⁹G. D. Kubiak, Surf. Sci. **201**, L475 (1988).

- ²⁰W. Steinmann and Th. Fauster, in *Laser Spectroscopy and Photochemistry on Metal Surfaces*, edited by H. L. Dai and W. Ho (World Scientific, Singapore, 1995), Chap. 5, p. 184.
- ²¹K. Giesen, F. Hage, F. J. Himpsel, H. J. Rieß, W. Steinmann, and N. V. Smith, *Phys. Rev. B* **35**, 975 (1987).
- ²²Th. Fauster, Ch. Reuß, I. L. Shumay, and M. Weinelt, *Chem. Phys.* **251**, 111 (2000).
- ²³E. Z. Luo, J. Wollschläger, F. Wegner, and M. Henzler, *Appl. Phys. A: Mater. Sci. Process.* **60**, 19 (1995).
- ²⁴F. Theilmann, Ph.D. thesis, Universität Kassel, 1998.
- ²⁵S. Schuppler, N. Fischer, Th. Fauster, and W. Steinmann, *Phys. Rev. B* **46**, 13 539 (1992); **47**, 10 058 (1993).
- ²⁶W. Wallauer, R. Fischer, and Th. Fauster, *Surf. Sci.* **364**, 297 (1996).
- ²⁷J. M. García, O. Sánchez, P. Segovia, J. E. Ortega, J. Alvarez, A. L. Vázquez de Parga, and R. Miranda, *Appl. Phys. A: Mater. Sci. Process.* **61**, 609 (1995).
- ²⁸O. Sánchez, J. M. García, P. Segovia, J. Alvarez, A. L. Vázquez de Parga, J. E. Ortega, M. Prietsch, and R. Miranda, *Phys. Rev. B* **52**, 7894 (1995).
- ²⁹X. Y. Wang, X. J. Shen, and R. M. Osgood, Jr., *Phys. Rev. B* **56**, 7665 (1997).
- ³⁰M. Weinelt, Ch. Reuß, M. Kutschera, U. Thomann, I. L. Shumay, Th. Fauster, U. Höfer, F. Theilmann, and A. Goldmann, *Appl. Phys. B: Lasers Opt.* **68**, 377 (1999).
- ³¹K. Morgenstern, G. Rosenfeld, E. Laegsgaard, F. Besenbacher, and G. Comsa, *Phys. Rev. Lett.* **80**, 556 (1998).
- ³²H. Brune, K. Bromann, H. Röder, K. Kern, J. Jacobsen, P. Stoltze, K. Jacobsen, and J. Nørskov, *Phys. Rev. B* **52**, R14 380 (1995).